

Observation of Coulomb blockade and Coulomb staircases in superconducting $\text{Pr}_{0.8}\text{Sr}_{0.2}\text{NiO}_2$ films

Rui-Feng Wang,¹ Yan-Ling Xiong,¹ Hang Yan,¹ Xiaopeng Hu,¹ Motoki Osada,^{2,3}
Danfeng Li,^{4,*} Harold Y. Hwang,^{2,3} Can-Li Song,^{1,5,†} Xu-Cun Ma,^{1,5,‡} and Qi-Kun Xue^{1,5,6}

¹*State Key Laboratory of Low-Dimensional Quantum Physics,
Department of Physics, Tsinghua University, Beijing 100084, China*

²*Stanford Institute for Materials and Energy Sciences,*

SLAC National Accelerator Laboratory, Menlo Park, California 94025, United States

³*Department of Applied Physics, Stanford University, Stanford, California 94305, United States*

⁴*Department of Physics, City University of Hong Kong, Kowloon, Hong Kong SAR 999077, China*

⁵*Frontier Science Center for Quantum Information, Beijing 100084, China*

⁶*Southern University of Science and Technology, Shenzhen 518055, China*

Motivated by the discovery of superconductivity in the infinite-layer nickelate family, we report an experimental endeavor to clean the surface of nickelate superconductor $\text{Pr}_{0.8}\text{Sr}_{0.2}\text{NiO}_2$ films by Ar^+ ion sputtering and subsequent annealing, and we study their electronic structures by cryogenic scanning tunneling microscopy and spectroscopy. The annealed surfaces are characterized by nano-sized clusters and Coulomb staircases with periodicity inversely proportional to the projected area of the nanoclusters, consistent with a double-barrier tunneling junction model. Moreover, the dynamical Coulomb blockade effects are observed and result in well-defined energy gaps around the Fermi level, which correlate closely with the specific configuration of the junctions. These Coulomb blockade-related phenomena provide an alternative plausible cause of the observed gap structure that should be considered in the spectroscopic understanding of nickelate superconductors with the nano-clustered surface.

I. INTRODUCTION

The recent discovery of the infinite-layer nickelate family $\text{R}_{1-x}(\text{Sr}, \text{Ca})_x\text{NiO}_2$ ($\text{R} = \text{Nd}, \text{Pr}, \text{La}$) has provided a fascinating platform for exploring electronic correlation and superconductivity in complex oxide materials [1–4]. Unlike their cuprate counterparts [5], the nickelates exhibit a distinct phase diagram without an insulating parent state [6–9], and are considered to possess a multi-orbital electronic structure [10–12]. Although surface-sensitive experimental techniques have proved powerful to clarify the electron pairing symmetry and inter-orbital interaction in high-temperature (T_c) superconductors [13, 14], they turn out to be challenging for the nickelate films because of the mandatory topotactic reduction process using CaH_2 , which may significantly degrade the top surface. A recent scanning tunneling microscopy/spectroscopy (STM/STS) study showed the strange coexistence of a V-shaped energy gap and a fully opened energy gap on a nano-clustered $\text{Nd}_{1-x}\text{Sr}_x\text{NiO}_2$ surface after a long-time vacuum annealing [15]. Despite several theoretical proposals [16–20], the origin of the two different types of energy gaps and the pairing symmetry of nickelate superconductors remain mysterious.

As is well known, the geometry of an object can profoundly affect the electronic properties as its dimensions are reduced to that comparable to characteristic length scales [21, 22]. Specifically, if the charging energy $e^2/2C$

(e is the electron charge and C is the capacitance) of a nano-sized object is larger than the energy of thermal fluctuations ($k_B T$) (k_B is the Boltzmann constant), the effect of single-electron tunneling (SET) arises. In widely studied systems such as metal nanoparticles [23–27] and discontinuous films [28], a double-barrier tunneling junction (DBTJ) model based on the orthodox theory provides a fairly good description of the experimental spectra [29–31]. Controlled by the impedance of the internal junctions, the tunneling current often exhibits equally spaced Coulomb staircases with increasing bias voltage. On the other hand, in a single junction dominating system, quantum fluctuations exert a significant influence on the SET and lead to a dynamic Coulomb blockade (DCB) [32, 33], yielding an energy gap near the Fermi level (E_F) [34, 35]. Here, we report such behaviors on the surface of superconducting $\text{Pr}_{0.8}\text{Sr}_{0.2}\text{NiO}_2$ (PSNO) films. Our results call for a more comprehensive understanding of the gap-like features of tunneling spectra on the nano-clustered surface of nickelate superconductors.

II. METHODS

The infinite-layer PSNO films were prepared on SrTiO_3 (STO) substrates by reducing the precursor $\text{Pr}_{0.8}\text{Sr}_{0.2}\text{NiO}_3$ thin films grown by the pulsed laser deposition, as detailed elsewhere [2]. Afterward, the samples were *ex situ* transferred to our UHV chamber connected to a Unisoku USM 1300 ^3He STM system. Prior to STM measurements, we cleaned the samples with Ar^+ ion sputtering at energies of 500~1000 eV for 10~45 minutes under a pressure of 1×10^{-5} Torr and then annealed

* danfeng.li@cityu.edu.hk

† clsong07@mail.tsinghua.edu.cn

‡ xucunma@mail.tsinghua.edu.cn

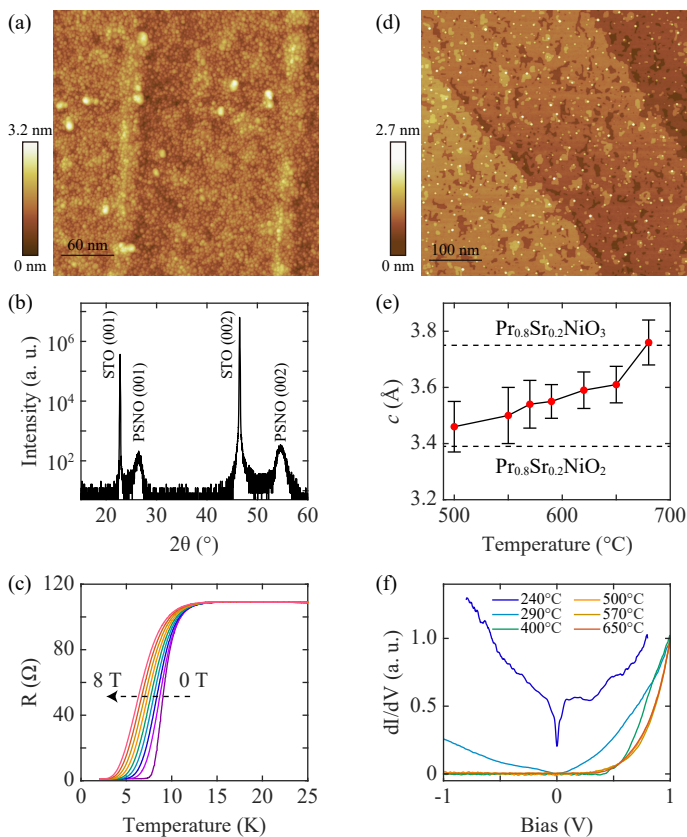


FIG. 1. (a) STM topographic image of PSNO after Ar^+ sputtering and annealing at 200°C ($300\text{ nm} \times 300\text{ nm}$, $V = -3.0\text{ V}$, $I = 10\text{ pA}$). (b) XRD pattern (wavelength of the X-ray: 1.5406 \AA) of PSNO after treatments at 200°C , showing the infinite-layer PSNO phase. (c) Temperature dependent resistance curves of the PSNO sample in (b) under varied magnetic fields. The superconducting onset temperature of 10.8 K is similar to the films before Ar^+ sputtering and annealing. (d) STM topographic image of PSNO after Ar^+ sputtering and annealing at 650°C ($500\text{ nm} \times 500\text{ nm}$, $V = 2.7\text{ V}$, $I = 10\text{ pA}$). (e) Step heights of PSNO films as a function of annealing temperatures. Each point comes from the measurements of 20 profiles, and the error bar indicates the standard deviation. (f) Spatially averaged dI/dV spectra measured at 4.2 K on the surface of PSNO samples after various annealing temperatures.

them in UHV to improve the crystalline quality at varied temperatures. Unless otherwise specified, the STM measurements were conducted at 0.4 K with a polycrystalline PtIr tip, which was cleaned by e -beam heating in UHV and calibrated on MBE-grown Ag/Si(111) films. Tunneling spectra were measured using a standard lock-in technique with a small bias modulation at 931 Hz .

III. RESULTS AND DISCUSSIONS

Figure 1(a) shows a typical STM topographic image of the PSNO films upon sputtering at 500 eV for 10 minutes

and annealing at 200°C for 1 hour. The film exhibits a corrugated surface covered with nano-sized clusters. This topography is highly reproducible for all PSNO samples under similar treatments. The samples retain the infinite-layer crystal structure and bulk superconductivity with a T_c^{onset} of 10.8 K (the temperature at which the resistance reduces to 90% of the value at 20 K), as confirmed by X-ray diffraction (XRD) [Fig. 1(b)] and macroscopic transport measurements [Fig. 1(c)]. This nano-clustered topography is little affected by further Ar^+ ion sputtering. However, it undergoes an evident transformation into an atomically flat step-terrace structure as the annealing temperature is increased above 500°C , as shown in Fig. 1(d). The step height gradually changes from near the c -axis length of the PSNO phase (3.39 \AA) to that of the $\text{Pr}_{0.8}\text{Sr}_{0.2}\text{NiO}_3$ phase (3.75 \AA) with increasing temperature [Fig. 1(e)]. Meanwhile, the tunneling spectra change from metallic characteristics to insulating ones [Fig. 1(f)]. We therefore focus on the spectral measurements on the nano-clustered surface after low-temperature annealing ($180\sim 240^\circ\text{C}$).

The PSNO nanoclusters are clearly imaged by a magnified STM image shown in Fig. 2(a). They are shaped as irregular polygons and mostly approximated as hemispheres. This allows us to measure their sizes by the diameter (labeled as d) of the outmost periphery of various nanoclusters. Figure 2(b) shows spatially resolved dI/dV spectra straddling various nanoclusters taken at 4.2 K . These spectra exhibit a remarkable size d dependence and can be divided into two categories. One is on the small nanoclusters that exhibits an energy gap around the Fermi level (E_F) and additional oscillatory peaks outside the low-energy gap. The other one is characteristic of a metal-like feature with an obvious spectral dip at E_F . To clarify the relationship between the spectra and the size of PSNO nanoclusters, we systematically measured the dI/dV spectra as well as effective diameters for various nanoclusters, as illustrated in Figs. 2(c) and 2(d). In general, all the spectra exhibit equidistant oscillatory peaks with increasing bias, reminiscent of Coulomb staircases for the single electron tunneling. According to this scenario, each peak means that the number of electrons in the nanoclusters changes by 1. As described in the DBTJ model [29–31], the barrier increases with the decrease of the nanocluster size via $E_C = e/C_2$, where C_2 is the effective capacitance between the nanocluster and the continuous film beneath it. Figure 2(e) shows the dependence of E_C on d for various nanoclusters, justifying an inversely quadratic relationship between them via $E_C \propto 1/d^2$, because the capacitance of a metal island is proportional to the projected area in scale with d^2 . Therefore, this result provides strong evidence for the notion that the equally spaced conductance peaks originate from Coulomb blockade effects in the PSNO nanoclusters.

Note that the equidistant conductance peaks of the tunneling dI/dV spectra hold true only for those well above and below E_F , whereas the energy spacing be-

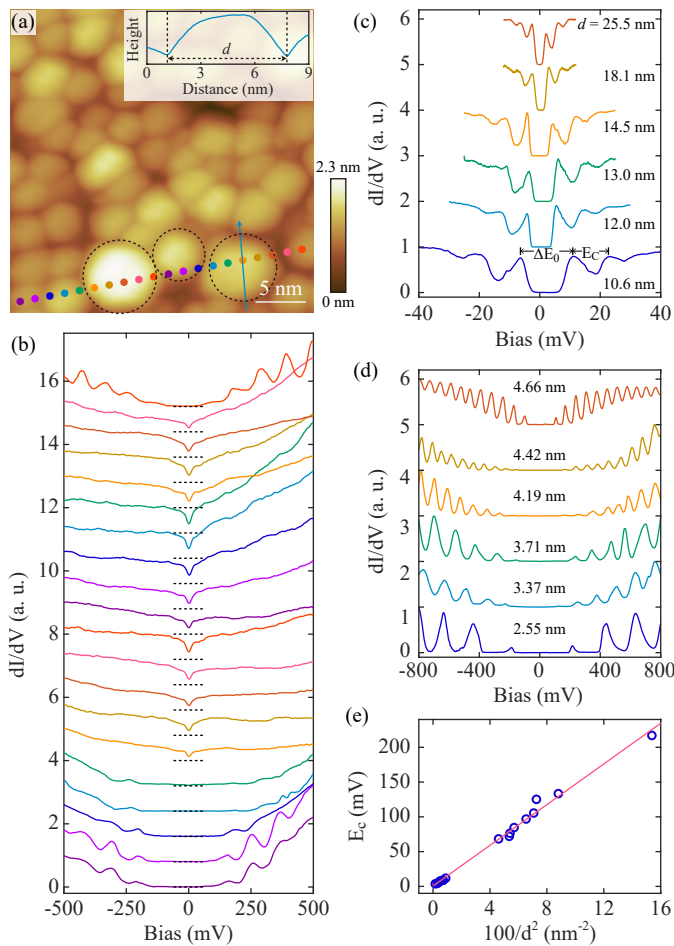


FIG. 2. (a) STM topographic image of PNSO nanoclusters ($30 \text{ nm} \times 30 \text{ nm}$, $V = -3.0 \text{ V}$, $I = 10 \text{ pA}$). The nanoclusters are marked by dashed circles with various effective diameters (d). Inset: line profile along the blue arrow to determine the d value. (b) A series of dI/dV spectra (set points: $V = -500 \text{ mV}$, $I = 100 \text{ pA}$) acquired on the correspondingly colored spots in (a). (c), (d) Representative spectra on the nanoclusters of different sizes, as labeled. The set points in (c) are $V = 40 \text{ mV}$, 30 mV , 25 mV , 25 mV , 12 mV , 12 mV , $I = 1.5 \text{ nA}$, 8.0 nA , 6.0 nA , 6.0 nA , 1.3 nA , 2.0 nA for the spectra from bottom up. The set points in (d) are $V = -800 \text{ mV}$, $I = 0.6 \text{ nA}$ for the 25.5-nm nanocluster and $V = -800 \text{ mV}$, $I = 1.0 \text{ nA}$ for other sized nanoclusters. (e) Relationship between Coulomb staircase periodicity (E_C) and size parameters $1/d^2$. The red curve shows the best linear fit between them.

tween the two peaks on both sides of E_F (labeled as ΔE_0) is commonly larger than E_C . A straightforward explanation may be that the gap ΔE_0 contains the superconducting gap (Δ_S) in PSNO. For most size-confined superconducting systems, the relationship $\Delta E_0 = E_C + 2\Delta_S$ holds when the cluster size exceeds the Anderson limit [27, 28, 36]. At elevated temperature or magnetic field, the superconducting gap is suppressed and the gap ΔE_0 will reduce from $E_C + 2\Delta_S$ to E_C , which provides a feasible criterion to distinguish superconductivity from the coupled Coulomb effect. To this purpose, temperature-

dependent spectral investigations have been carried out on two typical nanoclusters with $d = 12.0 \text{ nm}$ and $d = 25.5 \text{ nm}$ [Figs. 3(a)-3(d)], respectively. The extracted ΔE_0 and E_C from these spectra are shown in Figs. 3(b) and 3(d), where the E_C are extracted from the average of the energy differences between the first and second oscillatory peaks (marked by short rods) on both energy sides. Surprisingly, the gap ΔE_0 never approaches E_C with temperature, and the thermal broadening effect even broadens the two E_F -near conductance peaks such that ΔE_0 phenomenally increases with temperature. At elevated temperatures, the gap-like features and conductance peaks gradually weaken and eventually disappear at the same time. The closing temperature of ΔE_0 (6 K) in the 25.5-nm nanocluster is less than that (15 K) in the 12.0-nm nanocluster, which seems to be contradictory to the quantum size effect of superconductors that generally present a weaker superconductivity in smaller-sized nanoclusters [37]. Furthermore, we have also measured a series of dI/dV spectra on varying magnetic fields in Figs. 3(e) and 3(f), from which the extracted ΔE_0 and E_C change little with the increasing field. These results compellingly indicate that ΔE_0 completely originates from the Coulomb effect and gets smeared out at elevated temperatures. No clear signature of the superconducting gap is found from our careful spectral measurements on the nano-clustered surface, even though the bulk superconductivity of the samples has been confirmed by transport measurements. Our results suggest that the nano-clustered surface has different stoichiometry from the bulk of the PSNO superconductors, where more caution should be paid in interpreting the gap-like features in the nickelate system.

Having excluded the involved superconductivity, the DCB is considered as an alternative cause for the widened ΔE_0 . Experimentally, the DCB induced conductance gaps appear at high environmental impedance and are critically dependent on the tip-sample distances [34, 35]. To check this scenario, Fig. 4(a) shows a series of site-specific normalized tunneling spectra on a 25.5-nm nanocluster at varied current set points. Evidently, there exists only a gap ΔE_0 in the dI/dV spectra measured at $I \leq 0.5 \text{ nA}$, while the Coulomb staircases become more and more remarkable and ΔE_0 gradually decreases to E_C at larger I [Fig. 4(b)]. These results show a salient crossover from Coulomb blockade (a dominant single junction) to Coulomb staircases (double-barrier junctions). As illustrated in Fig. 4(c), the whole experimental setup can be simplified to two tunneling junctions, just as in the DBTJ model. The first junction is between the tip and the surface PSNO nanocluster with an effective resistance R_1 and capacitance C_1 , and the other one is between the surface PSNO nanocluster and the underlying PSNO film with effective parameters R_2 and C_2 . When the distance between the tip and the sample is large enough, where R_1 is much larger than R_2 , the first tunneling channel is dominant. However, as the tip approaches the sample surface so that R_1 is comparable

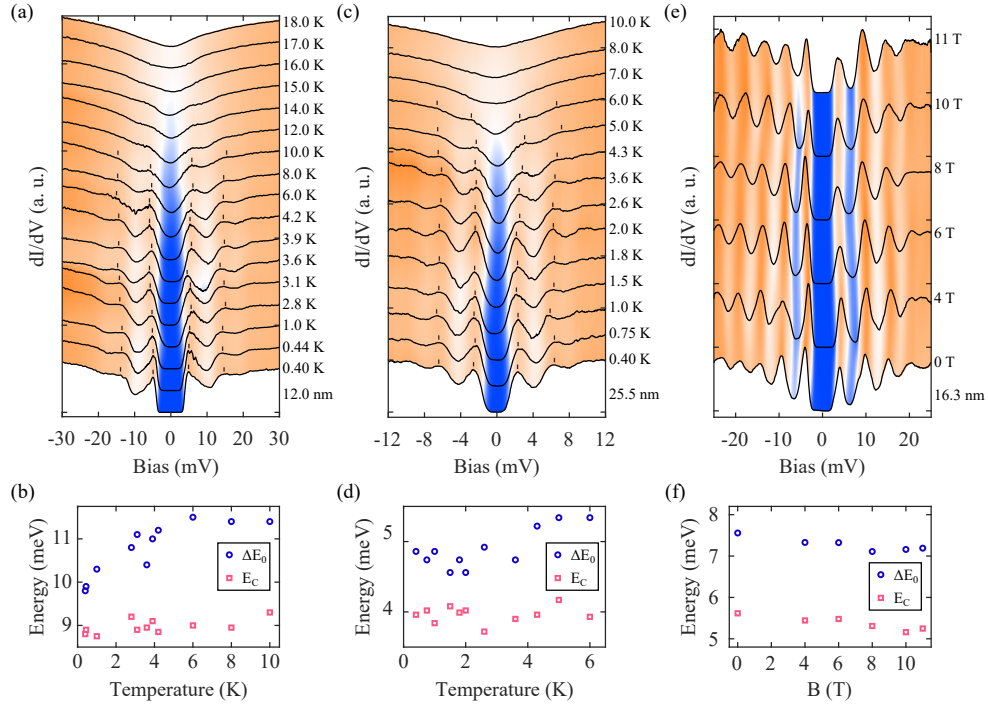


FIG. 3. (a) Temperature dependent dI/dV spectra (set points: $V = 30$ mV, $I = 8.0$ nA) measured in a 12.0-nm PSNO nanocluster. (b) The extract ΔE_0 and E_C of spectra in (a) as a function of temperatures. (c), (d) Same as (a), (b) but on a 25.5-nm PSNO nanocluster. The set points are $V = 12$ mV, $I = 2.0$ nA. (e) A series of dI/dV spectra (set points: $V = 25$ mV, $I = 4.0$ nA) measured in a 16.3-nm PSNO nanocluster under different magnetic fields. (f) The extract ΔE_0 and E_C of spectra in (e) as a function of magnetic fields.

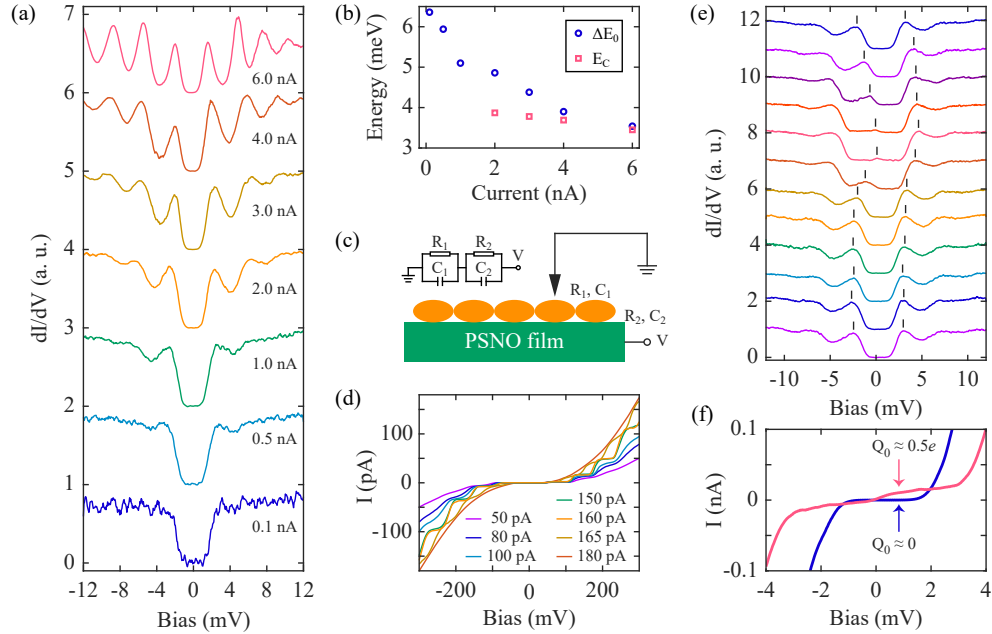


FIG. 4. (a) A series of dI/dV spectra on a 25.5-nm PSNO nanocluster as a function of tunneling current set points. The bias set points are stabilized at 12 mV. (b) The extract ΔE_0 and E_C as a function of the current set points. (c) Schematic illustration of the DBTJ model on the PSNO surface and equivalent circuit of this structure. (d) A series of I - V curves measured on a 4.66-nm PSNO nanocluster at different tunneling current set points. The bias set points are fixed at 300 mV. (e) A series of dI/dV spectra (set points: $V = 12$ mV, $I = 1.3$ nA) acquired along a trajectory of 8.0 nm in an 18.1-nm PSNO nanocluster. (f) Comparison of I - V curves between $Q_0 \approx 0$ and $Q_0 \approx 0.5e$.

with R_2 , the second tunneling channel comes into play and the double junctions jointly cause the equidistant oscillatory peaks with the periodicity $E_C = e/C_2$. In special conditions (e.g. $I = 6.0$ nA), the I - V spectrum exhibits equally spaced staircases and the dI/dV spectrum exhibits discrete peaks, where the influence of DCB is negligible. Figure 4(d) shows another series of measurements on a 4.66-nm nanocluster with larger R_2 . One can immediately notice that the similar Coulomb staircases happen only for intermediate tunneling current set points ($80 \text{ pA} \leq I \leq 165 \text{ pA}$). Too small or too large current set point I means $R_1 \gg R_2$ or $R_1 \ll R_2$, which changes the configuration to a single junction model dominated by the first or second tunneling junction.

In addition to the effective resistances and capacitances, the fractional residual charge Q_0 is another important parameter in the DBTJ model, which represents the effective initial charge in the central electrode. Figure 4(e) illustrates the influence of Q_0 via a series of Coulomb staircases along a trajectory of 8.0 nm in an 18.1-nm nanocluster. These spectra are not symmetric with respect to E_F but are shifted in energy because of the local variation of Q_0 . In principle, the locations of the first spectral peaks below and above E_F have analytical expressions $x_1 = (-e/2 + Q_0)/C_2$ and $x_2 = (e/2 + Q_0)/C_2$. As Q_0 approaches $e/2$, x_1 moves to the E_F with minimum intensity. Figure 4(f) exhibits magnified I - V spectra between $Q_0 \approx 0$ and $Q_0 \approx e/2$. At $Q_0 \approx 0$, the spectrum is characteristic of a Coulomb gap, while at $Q_0 \approx e/2$, the gap vanished and the I - V curve shows a nonzero slope everywhere. The residual charge is considered to originate from the site-varying work functions and capacitances of the junctions [29]. Given the almost identical shape of spectra beyond the first peaks, the capacitances should remain unchanged when the tip moves on the same nanocluster. Therefore, we ascribe the varying Q_0 to the variations of local work functions.

IV. SUMMARY

In conclusion, the Coulomb blockade and staircases have been clearly identified on the clean surface of superconducting PSNO thin films after Ar^+ ion sputtering and annealing treatments. The remarkable Coulomb staircases are investigated as a function of the nanocluster sizes, tip-sample distances, and residual charges, which corroborate a SET process described by the DBTJ model. More importantly, the crossover from Coulomb blockade to Coulomb staircases has been well evidenced. Our results reveal the significant Coulomb blockade effects that

should be carefully considered to explain the tunneling spectra of nano-clustered surface in infinite-layer nickelates.

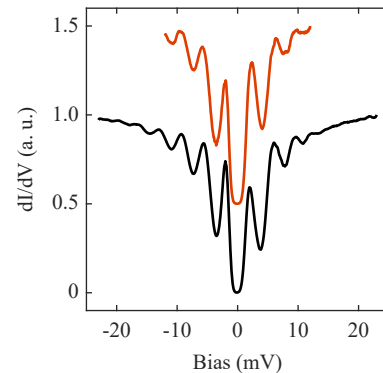


FIG. 5. Two dI/dV spectra measured on the same nanocluster with different energy ranges. The spectra are vertically shifted for clarity. The set points of the lower spectrum are $V = 23$ mV, $I = 8.0$ nA and those of the upper spectrum are $V = 12$ mV, $I = 3.0$ nA.

ACKNOWLEDGMENTS

The work at China was supported by the National Key R&D of China (Grant No. 2022YFA1403100), the National Natural Science Foundation of China (Grant No. 12134008). The work at Stanford/SLAC was supported by the US Department of Energy, Office of Basic Energy Sciences, Division of Materials Sciences and Engineering, under contract no. DE-AC02-76SF00515, and Gordon and Betty Moore Foundation's Emergent Phenomena in Quantum Systems Initiative through grant no. GBMF9072 (synthesis equipment). D.L. acknowledges the support from Hong Kong Research Grants Council (RGC) through ECS (CityU 21301221) and GRF (CityU 11309622) grants, and from National Science Foundation of China (NSFC12174325).

Appendix: Spectra at different energy scales

The oscillatory peaks from Coulomb staircases are obvious only when the effective resistances R_1 and R_2 satisfy an appropriate relationship, which makes us measure the dI/dV spectra at different set-point conditions. However, it should be emphasized that the period E_C does not change at a wide range of set points as long as the DBTJ forms [Figs. 4(a) and 4(d)]. To further validate this point, we show two dI/dV spectra at different energy scales in Fig. 5, where the spectrum at larger energy encompasses the oscillatory patterns of the one at smaller energy.

[1] Danfeng Li, Kyuho Lee, Bai Yang Wang, Motoki Osada, Samuel Crossley, Hye Ryoung Lee, Yi Cui, Yasuyuki

Hikita, and Harold Y Hwang, "Superconductivity in an infinite-layer nickelate," *Nature* **572**, 624–627 (2019).

- [2] Motoki Osada, Bai Yang Wang, Berit H Goodge, Kyuho Lee, Hyeok Yoon, Keita Sakuma, Danfeng Li, Masashi Miura, Lena F Kourkoutis, and Harold Y Hwang, “A superconducting praseodymium nickelate with infinite layer structure,” *Nano Lett.* **20**, 5735–5740 (2020).
- [3] Shengwei Zeng, Changjian Li, Lin Er Chow, Yu Cao, Zhaoting Zhang, Chi Sin Tang, Xinmao Yin, Zhi Shih Lim, Junxiong Hu, Ping Yang, *et al.*, “Superconductivity in infinite-layer nickelate $\text{La}_{1-x}\text{Ca}_x\text{NiO}_2$ thin films,” *Sci. Adv.* **8**, eabl9927 (2022).
- [4] Motoki Osada, Bai Yang Wang, Berit H Goodge, Shannon P Harvey, Kyuho Lee, Danfeng Li, Lena F Kourkoutis, and Harold Y Hwang, “Nickelate superconductivity without rare-earth magnetism: $(\text{La}, \text{Sr})\text{NiO}_2$,” *Adv. Mater.* **33**, 2104083 (2021).
- [5] Bernhard Keimer, Steven A Kivelson, Michael R Norman, Shinichi Uchida, and J Zaanen, “From quantum matter to high-temperature superconductivity in copper oxides,” *Nature* **518**, 179–186 (2015).
- [6] Danfeng Li, Bai Yang Wang, Kyuho Lee, Shannon P Harvey, Motoki Osada, Berit H Goodge, Lena F Kourkoutis, and Harold Y Hwang, “Superconducting dome in $\text{Nd}_{1-x}\text{Sr}_x\text{NiO}_2$ infinite layer films,” *Phys. Rev. Lett.* **125**, 027001 (2020).
- [7] Shengwei Zeng, Chi Sin Tang, Xinmao Yin, Changjian Li, Mengsha Li, Zhen Huang, Junxiong Hu, Wei Liu, Ganesh Ji Omar, Hariom Jani, *et al.*, “Phase diagram and superconducting dome of infinite-layer $\text{Nd}_{1-x}\text{Sr}_x\text{NiO}_2$ thin films,” *Phys. Rev. Lett.* **125**, 147003 (2020).
- [8] Motoki Osada, Bai Yang Wang, Kyuho Lee, Danfeng Li, and Harold Y Hwang, “Phase diagram of infinite layer praseodymium nickelate $\text{Pr}_{1-x}\text{Sr}_x\text{NiO}_2$ thin films,” *Phys. Rev. Mater.* **4**, 121801 (2020).
- [9] Kyuho Lee, Bai Yang Wang, Motoki Osada, Berit H Goodge, Tiffany C Wang, Yonghun Lee, Shannon Harvey, Woo Jin Kim, Yijun Yu, Chaitanya Murthy, *et al.*, “Character of the ”normal state” of the nickelate superconductors,” arXiv preprint arXiv:2203.02580 (2022), 10.48550/arXiv.2203.02580.
- [10] Lun-Hui Hu and Congjun Wu, “Two-band model for magnetism and superconductivity in nickelates,” *Phys. Rev. Res.* **1**, 032046 (2019).
- [11] Antia S Botana and Michael R Norman, “Similarities and differences between LaNiO_2 and CaCuO_2 and implications for superconductivity,” *Phys. Rev. X* **10**, 011024 (2020).
- [12] Mi-Young Choi, Kwan-Woo Lee, and Warren E Pickett, “Role of 4f states in infinite-layer NdNiO_2 ,” *Phys. Rev. B* **101**, 020503 (2020).
- [13] Øystein Fischer, Martin Kugler, Ivan Maggio-Aprile, Christophe Berthod, and Christoph Renner, “Scanning tunneling spectroscopy of high-temperature superconductors,” *Rev. Mod. Phys.* **79**, 353 (2007).
- [14] Jennifer E Hoffman, “Spectroscopic scanning tunneling microscopy insights into Fe-based superconductors,” *Rep. Prog. Phys.* **74**, 124513 (2011).
- [15] Qiangqiang Gu, Yueying Li, Siyuan Wan, Huazhou Li, Wei Guo, Huan Yang, Qing Li, Xiyu Zhu, Xiaoqing Pan, Yuefeng Nie, and Hai-Hu Wen, “Single particle tunneling spectrum of superconducting $\text{Nd}_{1-x}\text{Sr}_x\text{NiO}_2$ thin films,” *Nat. Commun.* **11**, 1–7 (2020).
- [16] Qiangqiang Gu and Haihu Wen, “Superconductivity in nickel based 112 systems,” *The Innovation* **3**, 100202 (2021).
- [17] Priyo Adhikary, Subhadeep Bandyopadhyay, Tanmoy Das, Indra Dasgupta, and Tanusri Saha-Dasgupta, “Orbital-selective superconductivity in a two-band model of infinite-layer nickelates,” *Phys. Rev. B* **102**, 100501 (2020).
- [18] Zhan Wang, Guang-Ming Zhang, Yi-feng Yang, and Fu-Chun Zhang, “Distinct pairing symmetries of superconductivity in infinite-layer nickelates,” *Phys. Rev. B* **102**, 220501 (2020).
- [19] Xianxin Wu, Kun Jiang, Domenico Di Sante, Werner Hanke, AP Schnyder, Jiangping Hu, and Ronny Thomale, “Surface *s*-wave superconductivity for oxide-terminated infinite-layer nickelates,” arXiv preprint arXiv:2008.06009 (2020), 10.48550/arXiv.2008.06009.
- [20] Peayush Choubey and Ilya M Eremin, “Electronic theory for scanning tunneling microscopy spectra in infinite-layer nickelate superconductors,” *Phys. Rev. B* **104**, 144504 (2021).
- [21] Johannes Antonius Albertus Joseph Perenboom, Peter Wyder, and Felix Meier, “Electronic properties of small metallic particles,” *Phys. Rep.* **78**, 173–292 (1981).
- [22] Konstantin K Likharev, “Correlated discrete transfer of single electrons in ultrasmall tunnel junctions,” *IBM J. Res. Dev.* **32**, 144–158 (1988).
- [23] Hong Zhang, Yuhsuke Yasutake, Yuhkatsu Shichibu, Toshiharu Teranishi, and Yutaka Majima, “Tunneling resistance of double-barrier tunneling structures with an alkanethiol-protected Au nanoparticle,” *Phys. Rev. B* **72**, 205441 (2005).
- [24] Shinya Kano, Tsukasa Tada, and Yutaka Majima, “Nanoparticle characterization based on STM and STS,” *Chem. Soc. Rev.* **44**, 970–987 (2015).
- [25] C Schönenberger, H Van Houten, and HC Donkersloot, “Single-electron tunnelling observed at room temperature by scanning-tunnelling microscopy,” *Europhys. Lett.* **20**, 249 (1992).
- [26] JGA Dubois, JW Gerritsen, SE Shafranjuk, EJG Boon, G Schmid, and H Van Kempen, “Coulomb staircases and quantum size effects in tunnelling spectroscopy on ligand-stabilized metal clusters,” *Europhys. Lett.* **33**, 279 (1996).
- [27] Jin Qin, Chenxiao Zhao, Bing Xia, Zerui Wang, Yu Liu, Dandan Guan, Shiyong Wang, Yaoyi Li, Hao Zheng, Canhua Liu, *et al.*, “Coupling of superconductivity and Coulomb blockade in Sn nanoparticles,” *Nanotechnology* **31**, 305708 (2020).
- [28] Yonghao Yuan, Xintong Wang, Canli Song, Lili Wang, Ke He, Xucun Ma, Hong Yao, Wei Li, and Qi-Kun Xue, “Observation of coulomb gap and enhanced superconducting gap in nano-sized Pb islands grown on SrTiO_3 ,” *Chin. Phys. Lett.* **37**, 017402 (2020).
- [29] AE Hanna and M Tinkham, “Variation of the Coulomb staircase in a two-junction system by fractional electron charge,” *Phys. Rev. B* **44**, 5919 (1991).
- [30] DV Averin, AN Korotkov, and KK Likharev, “Theory of single-electron charging of quantum wells and dots,” *Phys. Rev. B* **44**, 6199 (1991).
- [31] M Amman, R Wilkins, E Ben-Jacob, PD Maker, and RC Jaklevic, “Analytic solution for the current-voltage characteristic of two mesoscopic tunnel junctions coupled in series,” *Phys. Rev. B* **43**, 1146 (1991).
- [32] P Delsing, KK Likharev, Lo S Kuzmin, and T Claesson, “Effect of high-frequency electrodynamic environ-

- ment on the single-electron tunneling in ultrasmall junctions,” *Phys. Rev. Lett.* **63**, 1180 (1989).
- [33] Michel H Devoret, Daniel Esteve, Hermann Grabert, G-L Ingold, Hugues Pothier, and Cristian Urbina, “Effect of the electromagnetic environment on the Coulomb blockade in ultrasmall tunnel junctions,” *Phys. Rev. Lett.* **64**, 1824 (1990).
- [34] Christophe Brun, Konrad H Müller, I-Po Hong, François Patthey, Christian Flindt, and Wolf-Dieter Schneider, “Dynamical Coulomb blockade observed in nanosized electrical contacts,” *Phys. Rev. Lett.* **108**, 126802 (2012).
- [35] Jacob Senkpiel, Jan C Klöckner, Markus Etzkorn, Simon Dambach, Björn Kubala, Wolfgang Belzig, Alfredo Levy Yeyati, Juan Carlos Cuevas, Fabian Pauly, Joachim Ankerhold, *et al.*, “Dynamical Coulomb blockade as a local probe for quantum transport,” *Phys. Rev. Lett.* **124**, 156803 (2020).
- [36] Philip W Anderson, “Theory of dirty superconductors,” *J. Phys. Chem. Solids* **11**, 26–30 (1959).
- [37] Sangita Bose, Charudatta Galande, SP Chockalingam, Rajarshi Banerjee, Pratap Raychaudhuri, and Pushan Ayyub, “Competing effects of surface phonon softening and quantum size effects on the superconducting properties of nanostructured Pb,” *J. Phys. Condens. Matter* **21**, 205702 (2009).